Physiologically-Based Pharmacokinetic Models Can be used to Predict the Unique Nonlinear

Absorption Profiles of Vismodegib

Louis Lin, Matthew R Wright, Cornelis ECA Hop, and Harvey Wong

Faculty of Pharmaceutical Sciences, University of British Columbia, Vancouver, BC V6T 1Z3, Canada. (LL & HW) and Department of Drug Metabolism and Pharmacokinetic, Genentech, Inc., South San Francisco, CA, USA. (MRW & CECAH).

Running Title: Oral PBPK Modeling of Vismodegib

Author to whom correspondence should be addressed:

Harvey Wong, PhD

Faculty of Pharmaceutical Sciences, The University of British Columbia

2405 Wesbrook Mall, Vancouver, BC. V6T 1Z3, Canada

Phone: 604-822-4707

Fax: 604-822-3035

E-mail: harvey.wong@ubc.ca

Number of Pages: 45

Number of Tables: 5

Number of Figures: 8

Number of References: 53

Number of Words in Abstract: 249

Introduction: 810

Discussion: 1877

LIST OF ABBREVIATIONS:

AUC, area under the concentration-time curve; AUC_{0-24}, area under the concentration-time curve from time 0 to 24h postdose; AUC_{0-168}, area under the concentration-time curve from time 0 to 168h postdose; AUC_{ss}, area under the concentration-time curve at from time 0 to 24h postdose at steady-state; AUC_{0-inf}, area under the concentration-time curve from time 0 to infinity; Cl, clearance; Cl_{int}, intrinsic clearance; C_{max}, maximum concentration; t_{max}, time to maximum concentration; C_{ss}, mean plasma concentration level at steady state; C_{sol}, solubility in gastrointestinal tract segment; $C_{sol\_stomach}$, solubility in stomach compartment; C_{sol_IF}, solubility in intestinal compartment; C_p, concentration in plasma; C_{liv}, concentration in liver; f_u, fraction unbound; GIT, gastrointestinal tract; ke, elimination rate constant; ka, absorption rate constant; Kt, small intestinal transit rate constant; Kt.stom, gastric emptying rate constant; Kt.colon, colonic excretion rate constant; PBPK, physiologically based pharmacokinetic; PGF, permeation gradient factor; PK, pharmacokinetics; Q_h, blood flow rate; SI, small intestinal segment; Vd, volume of distribution; V/F, apparent volume of distribution after oral dose;

ABSTRACT

Predicting human pharmacokinetics (PK) during the drug discovery phase is valuable to assess

doses required to reach therapeutic exposures. For orally administered compounds, however, this

can be especially difficult since the absorption process is complex. Vismodegib is a compound

with unique nonlinear oral PK characteristics in humans. Oral physiologically-based

pharmacokinetic (PBPK) models were built using preclinical *in vitro* and *in vivo* data and

successfully predicted the oral PK profiles in rats, dogs, and monkeys. Simulated drug exposures

(AUC_{0-inf} and C_{max}), following oral administration were within 2-fold of observed values for the

dog and monkey, and close to 2-fold for the rat, providing validation to the model structure.

Adaptation of this oral PBPK model to humans, using human physiological parameters coupled

with predicted human PK, resulted in underpredictions of vismodegib exposure following both

single and multiple doses. When observed human PK was used to drive the oral PBPK model,

oral PK profiles in humans were well predicted with fold errors in predicted vs observed drug

exposures being close to 1. Importantly, the oral PBPK model captured the unique nonlinear,

non-dose dependent PK of vismodegib at steady-state. The mechanism responsible for

nonlinearity was consistent with oral absorption being influenced by nonsink permeation

conditions. We introduce a new parameter, the permeation gradient factor, to characterize the

effect of nonsink conditions on permeation. Using vismodegib as an example, we demonstrate

the value of using oral PBPK models in drug discovery to predict the oral PK of compounds with

nonlinear absorption characteristics in human.

SIGNIFICANCE STATEMENT

A physiologically-based pharmacokinetic model was built to demonstrate the value of these models early in the drug discovery stage for the prediction of human PK for compounds with unusual oral pharmacokinetics. In this study, our PBPK model could successfully capture the unique steady-state oral pharmacokinetics of our model compound, vismodegib. The mechanism for nonlinearity can be attributed to nonsink permeation conditions in vivo. We introduce the permeation gradient factor as a parameter to assess this effect.

INTRODUCTION

Predicting human pharmacokinetic (PK) behavior for investigational compounds in early discovery stages is critical to assessing doses required to achieve therapeutic drug exposures. For orally administered compounds, this can be especially difficult, as the gastrointestinal environment is dynamic and complex. One powerful prediction tool that can capture this complexity is physiologically-based pharmacokinetic (PBPK) modelling. Unlike traditional empirical models, PBPK models are mechanistic in nature, as they integrate physiological processes with drug properties to incorporate biological interactions with drugs, such as dissolution and metabolic enzyme kinetics, and experimental conditions, such as dosing under a fasted or fed state. (Jones *et al.*, 2012; Zhuang and Lu, 2016; Li *et al.*, 2017; Lin and Wong, 2017). In a typical PBPK model, organs are represented as anatomical compartments which are connected by systemic circulation carrying drug. A series of differential equations containing physiological parameters describe drug movement throughout the body. Combined with compound specific inputs, PBPK models can mathematically capture the interaction of drug and body to simulate the PK profile and study individual ADME (absorption, distribution, metabolism, excretion) processes or behaviors.

Applications of PBPK models guiding drug discovery and development have been reported in literature (Yamazaki *et al.*, 2011; Chung *et al.*, 2015; Jones *et al.*, 2015; Zhuang and Lu, 2016). However, their use is more common in early clinical development when more information on compounds are available and are frequently used in applications such as prediction of drug-drug interactions (Sager *et al.*, 2015; Grimstein *et al.*, 2019). When data is limited, such as in earlier stages of drug discovery, PBPK models are less refined, as they may

6

not have been fully validated to capture the mechanisms and assumptions necessary to describe a compound's PK (Jones *et al.*, 2015; Lin and Wong, 2017). When used for prediction of human oral PK from preclinical data, prediction performance was poor as indicated by the results of two large scale blinded evaluation studies where only 23% (Poulin *et al.*, 2011) or 37.2% (Margolskee *et al.*, 2017) of predictions of oral PK were considered reasonably accurate based on criteria set within the manuscripts.

Approved for the treatment of basal cell carcinoma in 2012, vismodegib is a low clearance, poorly soluble drug with unique nonlinear oral PK properties (Dlugosz *et al.*, 2012; Rudin, 2012). Compared to compounds exhibiting linear PK, vismodegib exhibits a significantly decreased time to reach steady-state, lower than expected steady-state concentrations, and less than dose proportional oral PK in humans and dogs (Wong *et al.*, 2010; Graham *et al.*, 2011). Specifically in humans, following a single oral dose, the half-life of vismodegib was reported to be approximately 12 days (Graham *et al.*, 2011). Under typical linear PK, steady-state concentrations should be achieved by 5-7 half-lives (60-84 days). However, in all PK studies reported, vismodegib reaches steady state by 7-14 days following once daily dosing (Graham *et al.*, 2011, 2012). Furthermore, average steady state concentration was approximately 5-fold lower than anticipated assuming linear PK. Finally, vismodegib exhibited less than dose proportional increases in exposure following single oral doses of 150 mg, 270 mg and 540 mg. However, steady-state vismodegib concentrations following multiple daily doses at these three doses were similar.

Similar unusual accumulation characteristics were observed in early multiple dose toxicity studies in dogs. Using a PBPK modeling approach, Wong *et al* (2010) was able to attribute this steady-state behavior to a nonsink permeation phenomenon. With nonsink permeation, the

concentration gradient of drug driving permeation across the intestinal membrane diminishes

with increasing dose, which decreases absorption. Vismodegib has poor solubility resulting in

low concentrations in the intestinal lumen, the driving concentration for drug permeation. In

addition, vismodegib exhibits very low clearance in dogs and in humans resulting in high levels

of unbound drug systemically which serves as the receiving end of the permeation concentration

gradient (Wong *et al.*, 2009; Graham *et al.*, 2011, 2012). Further, high systemic concentrations

were postulated to be required for biological activity (Wong *et al.*, 2011) and were observed

clinically. This led us to hypothesize that nonsink permeation may play a similar role in the oral

PK profile for humans.

In this retrospective study, we investigated whether an oral PBPK model that captures

nonsink permeation can be used to prospectively predict the unexpected oral PK of vismodegib

in humans. Oral PBPK models for vismodegib were constructed for rat, dog, and monkey to first

confirm if *in vivo* oral PK profiles can be predicted in preclinical species prior to human

predictions. Once confirmed in preclinical species, we assessed whether our model structure can

capture nonlinear oral PK characteristics described in humans, first with disposition parameters

extrapolated via allometry and then with observed IV dose data. The mechanisms driving

nonlinear behavior were then further examined. We aim to demonstrate the utility of employing

oral PBPK models in the drug discovery setting for prediction of oral PK in human for

compounds with unusual absorption characteristics.

MATERIALS AND METHODS:

Data Extraction

Data from PK studies in literature were extracted via WebPlotDigitizer (WebPlotDigitizer, Version 4.4, Ankit Rohatgi) (Rohatgi, Ankit, 2020). The intercoder reliability and validity of this software has been previously examined by Drevon *et al.*, 2017.

Preclinical Pharmacokinetics

Preclinical PK studies used in our study were previously reported (Wong *et al.*, 2009). For the intravenous PK studies in rats, dogs, and monkeys, three male animals of each species were given a single intravenous (IV) dose of 1 mg/kg vismodegib in 30%, 80%, and 80% polyethylene glycol (PEG 400), respectively. For oral PK, three male animals for each species were given an oral vismodegib dose at 5 mg/kg (rats), or 2 mg/kg (dogs and monkeys) formulated in 0.5% methylcellulose with 0.2% Tween 80. For all studies, sequential plasma samples were collected following drug administration and vismodegib plasma concentrations were determined by LC/MS/MS.

Clinical Pharmacokinetics

Vismodegib clinical PK data was obtained from literature sources (Graham *et al.*, 2011, 2012). Single dose PK data was obtained from a study where healthy female volunteers were given a single low IV tracer dose (10 µg) of ^{14}C-vismodegib in combination with a 150 mg vismodegib hard gelatin capsule. In this study, vismodegib levels in plasma were monitored up to 56 days (Graham *et al.*, 2012). Single dose and multiple dose PK data were obtained from a second study where 68 cancer patients received either 150, 270, or 540 mg oral doses of vismodegib as powder in capsule (Graham *et al.*, 2011). Patients received a single oral dose of

9

vismodegib with a subsequent 7-day monitoring period. This was followed by daily oral dosing

for the duration of treatment. Vismodegib plasma concentrations were digitized for up to 65 days.

PBPK Model Structure and Vismodegib Inputs

PBPK models were built for the rat, dog, monkey, and human, each with its own set of

physiological parameters derived from literature (see Physiological Data Inputs section) using

Simulation, Analysis, and Modeling II software (SAAM II v2.3, The Epsilon Group,

Charlottesville, VA, USA). The PBPK model structure (Figure 1) is a modification of an oral

PBPK model described by Wong *et. al*, (2010) to include a liver compartment. In the current

model, nine segments make up the gastrointestinal tract (GIT): one for the stomach, seven for the

small intestine, and one for the colon. Transit rate constants dictate the flow rate of drug through

the GIT. The intestines are assumed to be cylindrical tubes and thus, volume is calculated by

$\pi r^2 L$ and surface area is calculated by $2\pi r L$, where L is equal to the length of each section and r

is equal to the intestinal radius.

Each segment has a compartment for the undissolved and dissolved state. Dissolution is

based on the Noyes-Whitney Equation (Noyes and Whitney, 1897)

$$\frac{\mathrm{d}X_{solution}}{\mathrm{d}t} = \frac{3D}{\rho r h} \cdot (C_{sol} \text{-} C_{GIT}) \cdot X_{solid} \tag{1}$$

Where $X_{solution}$ is amount of dissolved drug at time t. D is the diffusion coefficient (10^{-4} cm^2/s), ρ

is the drug particle density (1.34 g/cm^3), r is the particle radius (20 μm), and h is the diffusion

layer thickness (20 μm). Dissolution is driven by the concentration gradient between the

solubility in the particular gastrointestinal tract segment (C_{sol}) and concentration of dissolved

drug in a particular segment ($C_{GIT} = X_{solution}/$ volume of segment). For the stomach, C_{sol} was set

to 490 μg/mL [$C_{sol\_stomach}$; solubility in stomach based on solubility in simulated gastric fluid]

10

and for the small intestine segments, C_{sol} was set to 3.0 µg/mL [C_{sol_IF}; solubility in the small

intestine based on solubility in FaSSIF from pH from 6.0-6.8]; (Wong *et al.*, 2010).

Dissolved drug in small intestine (C_{GIT}) is then subject to permeation into the liver

compartment based on equation 2:

$$\frac{dX_{solution}}{dt} = -P_{app} \cdot SA \cdot (f_{mono} \cdot C_{GIT} - f_u \cdot C_{liv}) \tag{2}$$

Where P_{app} is the permeability coefficient, (set at 60.1 x 10^{-6} cm/s as previously reported; Wong

et al, 2010), *SA* is effective surface area of intestinal segment, f_{mono} is the fraction of compound

not in micelles, f_u is the free fraction of drug in the liver (f_u in plasma was used as surrogate) ,

and C_{liv} is drug concentration in the liver or liver blood. f_{mono} is a constant equivalent to aqueous

solubility ($C_{solBuffer}$ = 0.4 µg/mL) divided by solubility in simulated intestinal fluid (C_{sol_IF} = 3.0

µg/mL based on FaSSIF solubility) (Sugano *et al.*, 2007; Wong *et al.*, 2010). Unbound fraction

values were taken from plasma protein binding studies using equilibrium dialysis reported in

literature (Wong *et al.*, 2009). Effective surface area (SA) was calculated by the multiplying the

surface area by 450, which is the reported intestinal amplification factor as a result of the villi

and microvilli presence (Ferraris *et al.*, 1989). The permeation gradient was designated as the

concentration gradient between free drug in the intestinal lumen ($f_{mono}*C_{GIT}$) and unbound

concentration in in the liver ($fu*C_{liv}$) because vismodegib is highly permeable and has very low

intrinsic clearance (Wong *et al.*, 2009).

The maximum amount of dissolved compound not in micelles available for permeation is

dictated by aqueous solubility ($C_{solBuffer}$). Therefore, when $f_{mono} \cdot C_{GIT} > C_{solBuffer}$, permeation is

governed by equation 3:

$$\frac{dX_{solution}}{dt} = -P_{app} \cdot SA \cdot (C_{solBuffer} - f_u \cdot C_{liv}) \tag{3}$$

11

After permeation into the liver compartment, the rate of elimination of amount of vismodegib in liver (X_{liv}) and transfer to and from the central compartment described by equation 4:

$$\frac{dX_{liv}}{dt} = Q_h C_p - Q_h C_{liv} - f_u \cdot C_{liv} \cdot Cl_{int} \tag{4}$$

Where C_p is the concentration in the central compartment (plasma concentration), Q_h is hepatic blood flow, and Cl_{int} is intrinsic clearance.

For preclinical species, intrinsic clearance was back-calculated using reported *in vivo* clearance (Cl) from single IV dose data, *in vitro* f_u values and physiological hepatic blood flow (Q_h) data (see Physiological Data Inputs section), according to the following equation for the well-stirred model:

$$Cl = \frac{(f_u \cdot Cl_{int}) \cdot Q_h}{(f_u \cdot Cl_{int}) + Q_h} \tag{5}$$

In the preclinical PK report by Wong et al (2010), the authors also extrapolated predicted human values of volume of distribution (Vd) and clearance via allometry from mice, rats, dogs, and monkeys and these values were used as initial estimates for clinical simulations. Clearance predicted using allometry was estimated with and without the cynomolgus monkey by Wong *et al,* (2009) as there seemed to be differences in the rate of metabolism for monkeys. Metabolic stability in hepatocytes with a 3-hour incubation was high in all species tested (≥88% remaining) with the exception of the monkey where vismodegib was moderately stable (41% remaining). Allometry does not perform well when there are species differences in the rate of metabolism (Lin, 1998; Huang and Riviere, 2014). Therefore, the predicted clearance without monkey was used for our initial clinical simulations. Observed Vd and Cl from a clinical study where a single IV dose was administered were used for subsequent clinical simulations (Graham *et al.*, 2012).

12

Nonsink permeation was analyzed by the permeation gradient factor (PGF),

defined as

(6)

$$PGF = \frac{f_{mono} \cdot C_{GIT} - f_u \cdot C_{liv}}{f_{mono} \cdot C_{GIT}}, when\ eq.2\ is\ used\ for\ permeation$$

(7)

$$PGF = \frac{C_{solBuffer} - f_u \cdot C_{liv}}{f_{mono} \cdot C_{GIT}}, when\ eq.3\ is\ used\ for\ permeation$$

In which we assume a PGF of $0.67 - 1.0$ indicates sink and PGF < 0.67 indicates nonsink

permeation. The criteria was chosen to resemble sink condition requirements in dissolution

testing, for which concentration in the dissolution medium must remain under 1/3 of the

saturation solubility (Jamzad and Fassihi, 2006; Liu *et al.*, 2013). The effect of nonsink

conditions was also examined with a sink permeability model in which the concentration

gradient is omitted from the permeation.

$$\frac{dX_{solution}}{dt} = -P_{app} \cdot SA \cdot (f_{mono} \cdot C_{GIT}) \quad (8)$$

Physiological Data Inputs

Our rat, dog, monkey, and human PBPK models were modeled after a 0.25 kg Sprague

Dawley, a 9.0 kg beagle, a 3.5 kg cynomolgus, and a 70 kg man, respectively. Body weights in

preclinical species were selected to match those of the animals from the preclinical PK study,

despite being different from the average body weights in the literature data sources for the dog

(10 kg) and monkey (5 kg) (Davies and Morris, 1993; Wong *et al.*, 2009). To address this,

hepatic physiological parameters were body weight normalized. Due to limited data on

physiology specific to the cynomolgus monkey in literature, physiological data for rhesus

monkeys were also included and body weight normalized. Species specific model inputs are

given in Table 1.

13

PBPK Model Simulations

PBPK models for rat, dog and cyno were used to simulate an IV dose which was compared to the observed plasma concentration-time profiles. These models were then used to simulate PO concentration-time profiles. Maximum concentration (C_{max}), time to maximum concentration (t_{max}), and drug exposure, indicated by area under the concentration-time curve extrapolated to infinity (AUC_{0-inf}), were evaluated and compared to observed values for validation of preclinical models (see Model Evaluation section). AUC values were calculated by non-compartmental analysis via trapezoidal method (Gibaldi and Perrier, 1982).

In clinical simulations, Vd and Cl values from both allometry and observed clinical trials were used to predict PO concentration-time profiles from single dose and multiple dose data. AUC values from 24-hour periods were calculated for day 1 (AUC_{0-24}) and day 100 (AUC_{ss}) profiles. Simulations out to 100 days ensured steady-state levels. Steady-state concentrations (C_{ss}) were then calculated by dividing AUC_{ss} by tau (24 hours). Comparisons between observed versus predicted PK parameters were performed as described in the Model Evaluation Section below. Time to steady state is marked as the day when concentration levels first reach 95% C_{ss}.

One Compartment Model Simulation

A one compartment model was built for each dose in humans using Simulation, Analysis, and Modeling II software (SAAM II, The Epsilon Group, Charlottesville, USA). The elimination rate constant (ke) was determined to be 0.00216 h^{-1} from both the terminal phase of a single PO 150 mg dose and the terminal phase from a single IV 10 μg dose (Graham *et al.*, 2012). The absorption rate constant (ka) from a single PO dose of 150 mg was then fitted to obtain a value

of 0.243 h^{-1}. As ka and ke could not be estimated from fitting for all doses, these parameters were then fixed and the apparent volume of distribution after oral dose (V/F) fitted for each dose. The single compartment models were then simulated to 100 days to steady-state.

Model Evaluation

Predictive performance was considered successful if predicted and observed PK parameters were within a 2-fold error ratio

$$Fold\ Error = \frac{predicted}{observed}\ , if\ predicted > observed \tag{9}$$

$$Fold\ Error = \frac{observed}{predicted}\ , if\ observed > predicted \tag{10}$$

Where a ratio of 1.0 – 2.0 is considered within 2-fold error. In single dose comparisons, the C_{max}, t_{max}, and area under the concentration-time curve from 0 h to 168 h postdose (AUC_{0-168}) were compared. In multiple dose comparisons, the maximum steady-state concentration and steady state AUC_{0-24} were compared. A one-compartment model simulation was used to evaluate PBPK simulations for comparison of our PBPK model results against a traditional linear PK model.

The fit of the simulated concentration-time curve shape was assessed by lineshape analysis (equation 11), which functionally calculates the absolute average fold error (as defined by equations 9 and 10) of all observed and simulated time points for each animal species (Peters, 2008).

$$Lineshape\ Fold\ Error = 10^{[\frac{1}{n}\sum \log(Fold\ Error)]} \tag{11}$$

In the clinical models, time points from 0 h to 168 h were evaluated for the single dose and time points from 168 h until the end of the simulation were evaluated for the multiple dose studies.

15

RESULTS

Preclinical Simulations

Plasma concentration versus time plots for observed concentrations and the preclinical

simulation results is shown in Figure 2 and a comparison of the observed vs. simulated PK

parameters are shown in Table 2. Generally speaking, our models showed good performance for

both IV and PO profiles with predicted $AUC_{0\text{-inf}}$ and C_{max} being within 2 fold or less when

compared to observed values. The lineshape analysis of the concentration-time curves resulted in

average fold errors of 6.09, 1.28, and 2.07 for the rat, dog, and monkey PO PBPK models. The

high error in the rat PO model can likely be attributed to the apparent difference in half-life

between the observed IV profile and the observed PO profile (Figure 2 A-B), with the half-life

calculated from the last 3 points in each being 1.4 h and 2.4 h, respectively. Since the clearance

parameters were derived from the IV dose cohort, this discrepancy resulted in a large fold error

in the last two time points for the PO profile. Despite this, the rat oral $AUC_{0\text{-inf}}$ was only slightly

under-predicted and out of 2-fold error range (2.22) (Table 2).

Overall, the agreement between predicted and observed profiles and parameters indicated

good predictive performance following intravenous administration but more importantly oral

absorption in all three preclinical species and thus provided some validation for the PBPK model

for the use of the model to predict oral PK in humans.

Clinical Simulations

Simulation results from our PBPK model populated with preclinical predictions of human

PK are shown in Figure 3 and Table 3. Using predicted Vd and Cl_{int} derived from predicted Cl

(extrapolated using allometry) to drive the PBPK model resulted in an underprediction of human

oral PK in both single and multiple dose simulations. Predicted AUC_{0-168} from a single PO dose

was 105 μM*h, with a fold error of 4.59. For AUC_{ss} in multiple dose simulations, predicted fold

errors were 3.90, 2.39, and 1.91 for 150 mg, 270 mg, and 540 mg, respectively. Similarly,

average fold errors in the lineshape analysis all fell outside of the 2-fold range. Furthermore,

dose-dependent exposure was seen in steady-state simulations unlike what was observed for the

clinical oral PK where both C_{max} and AUC_{ss} were comparable at all 3 doses.

We recognize that predictions of human PK from preclinical allometry may be inaccurate.

As the main assumption is that Vd and Cl are proportional to body weight, allometry overlooks

any species differences that may play a role in a compound's PK. Therefore, in order to reduce

prediction error from allometric scaling and test the ability of our oral PBPK model to capture

the unique nonlinear steady-state characteristics of vismodegib, we performed oral PK

simulations using Cl_{int} derived from reported Cl and reported Vd in humans (Graham *et al.*, 2012)

to drive the model. Oral simulations using observed PK, performed significantly better when

simulating single and multiple dose oral PK (Figure 4). Steady-state characteristics were all

within 2-fold error (Table 4). We performed simulations by fitting single dose oral PK profiles at

150, 270 and 540 mg to a one-compartment model with oral dosing (Figure 5). This was

followed by multiple dose simulations using the dosing regimens used the clinical trials. These

simulations were performed in order to provide a reference for multiple dose steady-state

accumulation under linear PK conditions. Steady-state simulations predicted a higher than

observed accumulation (Figure 5 and Table 5). This overprediction of accumulation is more

prominent in the 270 and 540 mg simulations where the fold error is greater than 5 for both C_{max}

and AUC_{ss}. Additionally, the time to steady-state was approximately 60 days, which is consistent

with the assumption of approximately five half-lives under linear kinetic behavior ($t_{1/2}$ is ~ 12

17

hours; Graham *et al.*, 2012). More importantly, in contrast to steady-state simulations using the one-compartment model, the PBPK model was able to capture the nonlinear steady-state PK behaviors of vismodegib following oral dosing namely: 1) earlier than expected time to steady-state; 2) lower than expected accumulation; 3) lack of dose dependency at steady-state. For the PBPK simulations at 150, 270, and 540 mg that used Cl_{int} derived from observed Cl and observed Vd to drive the PBPK model, vismodegib concentrations reached steady-state within 8-17 days rather than at 5-7 half-lives (~60-84 days) as would be anticipated assuming linear PK. The accumulation ratio was 7.11, 5.45, and 3.94 for the 150, 270, and 540 mg multiple dose steady-state simulations rather than 23.8 anticipated assuming linear PK that was derived from simulations using the one-compartment model. Finally, consistent with observed data, increasing exposure with increasing dose was predicted following a single dose with the PBPK model (Table 4). However, following multiple doses, C_{ss} were comparable (21-26 μM) for all three doses and lacked dose dependency which is consistent with what was observed clinically (mean observed C_{ss} around 20 μM across 150 mg, 270 mg, and 540 mg cohorts; Graham *et al.*, 2011).

The PGF is an index of the concentration gradient between unbound intestinal and unbound systemic concentrations which drives permeation. If oral absorption is under complete sink conditions, absorption would be driven by the free intestinal concentrations which would be associated with a PGF value of 1. As unbound systemic concentrations of drug increase, PGF will decrease causing a decrease in absorption due to nonsink conditions increasingly becoming more prevalent. We consider a PGF ≤0.67 to be considered nonsink conditions. This criteria was chosen to resemble that for nonsink conditions in dissolution testing (Jamzad and Fassihi, 2006; Liu *et al.*, 2013). Analysis of PGF following oral administration of vismodegib for a single dose

18

and for multiple-doses to steady-state using the PBPK model driven by observed PK reveals declines in PGF especially under steady-state conditions, during which PGF remains under 0.07 for the entire dosing interval (Figure 6). This analysis suggests that under steady-state conditions, the concentration gradient that drives oral absorption is non-existent providing a plausible explanation for the unique oral PK of vismodegib.

In studying the absorption characteristics for vismodegib in humans, we altered our oral PBPK model by creating sink conditions where permeation was driven solely by unbound intestinal concentrations of vismodegib ($f_{mono} * C_{GIT}$) as shown in Equation 7. The results of this comparison for 150 mg daily dose are shown in Figure 7. As can be observed in Figure 7, an oral PBPK model containing a permeation gradient is required to describe the observed oral PK of vismodegib in humans. Finally, results from a sensitivity analysis examining the role of intestinal solubility on vismodegib absorption indicate that there are minimal increases in steady-state concentrations when intestinal solubility was increased from 3.0 µg/mL to 5.0 µg/mL and from 5.0 µg/mL to 10 µg/mL (Figure 8). There was no change in steady-state concentrations at solubility values higher than 10 µg/mL, leading to the conclusion that intestinal solubility limitations play a minor role in the steady-state absorption of vismodegib.

DISCUSSION

Accurately predicting the human oral PK of compounds being advanced into clinical development can help guide clinical trials and inform dosing strategies for optimal drug exposure. However, the prediction of human oral PK can be challenging due to the dynamic complex interactions involving drug properties and physiology, particularly for poorly soluble compounds. A mathematical approach that can mechanistically integrate preclinical data alongside with physiological data in order to simulate a predicted human concentration-time profiles is PBPK modeling. However most applications of oral absorption PBPK modeling are retrospective in nature (Zhang *et al.*, 2017). The reasons for this may be in the knowledge gaps surrounding the complex oral absorption processes, as highlighted by several large-scale evaluation studies on the use of PBPK models in predicting human oral PK (Poulin *et al.*, 2011; Darwich *et al.*, 2017). In most cases, bioavailability was under-predicted for poorly soluble compounds. Despite this, there are cases that demonstrate successful predictions of the extent of absorption from preclinical data (Yamazaki *et al.*, 2011; Parrott *et al.*, 2013; Matsumura *et al.*, 2020). In one example, predictive performance was shown to be better in a PBPK model compared to a one-compartment model using Cl and Vd estimated from allometric scaling (Yamazaki *et al.*, 2011). The knowledge gap in our understanding of oral absorption highlights the importance of validating PBPK models with preclinical *in vivo* data prior to attempts to predict oral PK in humans. Our current study aims to evaluate the use of oral PBPK models in the prediction of oral PK in preclinical species and in humans during drug discovery for a compound with unique nonlinear absorption characteristics.

The oral single dose PK of vismodegib in rat, dog and monkey was captured by our PBPK model providing a degree of validation to the model structure (Figure 2 and Table 2).

However, the initial PBPK predictions using predicted human Cl and Vd derived from preclinical data were poor for both single and multiple dose data (Figure 3 and Table 3). The failure in the initial simulations were due to discrepancies between the predicted and observed human PK parameters Cl and Vd of vismodegib.

Vismodegib is a very low clearance compound in humans (LoRusso *et al.*, 2011) and predicting clearance for these compounds are often difficult. Estimation of hepatic clearance in humans using *in vitro* metabolic stability assays in hepatocytes, is challenging as enzyme degradation that occurs in incubations longer than 3-hours presents a practical challenge to measurement of intrinsic clearance of highly metabolically stable compounds. For vismodegib, hepatocyte stability assays showed 96% remaining after a 3-hour incubation, which after considering potential analytical error, demonstrated virtually no turnover (Wong *et al.*, 2009). These challenges in characterization of hepatic clearance using standard hepatocyte incubations have been recognized and assay modifications have been reported in an attempt to increase resolution by prolonging assay time (Di *et al.*, 2012; Di and Obach, 2015). Predictions of human Cl using allometry, despite suggesting that the compound was low clearance in humans was successful categorically but unsuccessful quantitatively as the observed clearance in humans was approximately 9.3 fold lower (predicted 403 mL/h, observed 43.4 mL/h) (Wong *et al.*, 2009; Graham *et al.*, 2012). As simple allometry is an empirical extrapolation model that assumes parameters are proportional to body weight, it is an imperfect prediction tool that overlooks species differences in PK related mechanisms (Boxenbaum, 1984). Advances in the prediction of human Cl for low clearance compounds would serve to greatly benefit human PK predictions.

Model prediction was significantly improved when the human oral PBPK model was driven using the observed Vd and Cl_{int} derived from the observed Cl from a single IV dose study

in humans (Graham *et al.*, 2012). When comparing steady-state predictions from multiple dose simulations using a one-compartment model (Table 5), our PBPK predictions at steady-state following multiple doses were more accurate, with predictions from all doses examined having fold errors close to 1 (Table 4). Moreover, the oral nonlinear characteristics of vismodegib at steady-state were captured, indicated by a less than dose-proportional increase in exposure at steady-state with steady-state being reach at approximately 8-17 days and observed concentrations at steady-state being ~20 µM for all three doses simulated. These predictions were in line with the clinical observations. The improved prediction not only indicated the ability of our oral PBPK model to capture observed oral absorption characteristics of vismodegib but also the ability to use the PBPK model to further investigate the mechanisms driving the nonlinear oral PK of vismodegib.

A recent study explored the mechanisms of these characteristics in vismodegib with PBPK models (Dolton *et al.*, 2020). Similar to our findings, their model describing vismodegib oral PK in humans suggested that transport across the unstirred boundary layer between intestinal luminal fluid and enterocytes was rate limiting to absorption as the concentration gradient driving absorption declined with both increase in dose and dosing frequency. As suggested by our simulations examining PGF, at steady-state, the concentration gradient driving vismodegib absorption is very small (Figure 6). Our simulations where absorption was driven directly by unbound vismodegib concentrations in the intestinal fluid alone (Figure 7) illustrate that including the nonsink permeation mechanism is needed to describe vismodegib nonlinear PK.

At first glance, the nonlinear PK profile for vismodegib at steady-state could be attributed to other mechanisms, such as dissolution or solubility rate limited absorption, which are common

for poor solubility compounds. Both dissolution and solubility rate limited absorption are dependent on drug solubility in intestinal fluid where an increase in drug solubility in intestinal fluid would result in an increase drug exposure. In order, the investigate if dissolution or solubility rate limited absorption contributes to vismodegib's nonlinear behavior, we performed a sensitivity analysis where the solubility in intestine fluid is increased 10-fold ($C_{sol\_IF} = 3.0 - 30$ µg/mL). The results presented in Figure 8 show that a 10-fold increase in solubility provide very little improvement in systemic exposure at steady-state (Figure 8).

Another potential mechanism for less than predicted accumulation of vismodegib at steady-state is autoinduction, in which a drug induces or upregulates metabolic enzymes responsible for its elimination. However, in vitro studies indicated that vismodegib does not interact with the pregnant X receptor that leads to induction, nor does it induce CYP1A2, CYP2B6, or CYP3A4/5 in cultured human hepatocytes which implies a lack of interaction with AhR, CAR, and PXR, respectively (LoRusso et al., 2013). Further, in a clinical drug-drug interaction study, co-administration with vismodegib did no cause a change in the PK of oral contraceptives (norethindrone 1 mg/ethinyl estradiol 35 lg; CYP3A4 substrate) which confirms that CYP3A4 is not induced by vismodegib (LoRusso et al., 2013). Based on the totality of the data, it is unlikely that autoinduction is responsible for vismodegib's nonlinear PK characteristics as vismodegib does not appear to induce metabolic enzymes/transporters showing no signs of interaction with nuclear hormone receptors.

The permeation equation (Equation 2) can provide insight into why vismodegib may be susceptible to nonsink permeation. The concentration gradient driving absorption is calculated by the difference between intestinal free monomer concentration and unbound systemic concentrations. As intrinsic clearance is the intrinsic ability of the liver to eliminate unbound

drug (Benet and Zia-Amirhosseini, 1995), unbound vismodegib systemic concentrations are inherently higher due to the low intrinsic clearance of free drug leading to drug accumulation. Additionally, the upper limit of free monomer concentrations available for permeation is the aqueous solubility (Sugano *et al.*, 2007), which is also low (0.4 µg/mL). Therefore, we believe that it is the combination of these two drug properties that causes nonsink permeation leading to nonlinear PK, by effectively impeding the permeation gradient by increasing unbound systemic concentrations and decreasing free intestinal concentrations. An important distinction is that dissolved drug in the intestine available for permeation is drug that is not associated with micelles formed in the intestine but rather free drug in aqueous intestinal fluid. Consequently, when unbound systemic concentrations rise and reaches the solubility of vismodegib in aqueous intestinal fluid (represented by aqueous solubility), one would anticipate that drug could enter the intestine from the systemic circulation once free intestinal concentrations are lower than unbound systemic concentrations. This condition would be fulfilled when the oral vismodegib dose is transited down the intestinal tract. It should also be noted that nonsink permeation was also observed in dogs for vismodegib at steady-state, likely due to the similarly low clearance as in humans (Wong *et al.*, 2010). Further, dogs receiving an IV dose of vismodegib saw a rapid decline in systemic concentrations following an oral administration of activated charcoal. Charcoal acts to decrease intestinal vismodegib concentrations indicating that movement of drug from the systemic circulation to the intestinal compartment is possible when the permeation gradient is reversed.

To our knowledge, nonsink permeation has only been directly demonstrated in vivo for one compound, 1,3-dicyclohexyl urea (DCU), which also has poor aqueous solubility (Chiang *et al.*, 2013). In this study, rats that were administered an oral dose of DCU with an infusion of

deuterated DCU (D8-DCU) had lower systemic DCU concentrations than those that were given

oral DCU alone. This study provides evidence that high systemic concentrations of D8-DCU

administered by infusion, limited the absorption of orally administered DCU, by effectively

reducing the DCU permeation gradient across the intestinal wall. It is possible that other

compounds may also exhibit this type of nonlinear absorption behavior, especially those with

similarly very low solubility and very low clearance, and that the nonlinear absorption of these

other compounds are erroneously attributed to saturable absorption due to poor solubility.

Distinguishing these mechanisms may be important, as the approach to increase absorption is

different for each. For example, if nonlinearity in oral PK is due to dissolution rate limited

absorption of a poorly soluble compound, reductions in particle size will help improve steady-

state exposures (Sugano *et al.*, 2007) which would not the case for the nonsink permeation

mechanism. Understandably, nonsink permeation may be difficult to examine *in vivo*. Rather, it

may be more practical to investigate this phenomenon using a modeling approach.

We acknowledge the role of saturable binding to alpha-1-acid glycoprotein (AAG) in the

nonlinear PK of vismodegib and recognize this as a limitation of the current PBPK model

(Graham *et al.*, 2011; LoRusso *et al.*, 2011; Lu *et al.*, 2015; Dolton *et al.*, 2020). In this study,

we aimed to validate current PBPK model structure which can capture nonsink permeation in

preclinical species and see if we could predict human pharmacokinetics. The incorporation of a

plasma protein binding into the current absorption model to further examine mechanisms driving

vismodegib PK in humans and its variability is the focus of a future investigation.

Overall, our prospective oral PBPK model was able to predict the oral PK of vismodegib

well in preclinical species. Despite inadequate predictions in oral PK in humans when using Cl_{int}

derived from predicted Cl and predicted Vd, when the observed PK from IV dose data was used

to drive the PBPK model, the nonlinear oral PK was nicely captured. Using our mechanistic

PBPK model, we were then able to examine the effect of nonsink permeation on vismodegib PK.

The results of our study demonstrate the value in the use of oral PBPK models in predicting

unique oral absorption characteristics in humans in drug discovery, using vismodegib as a model

compound.

ACKNOWLEDGEMENTS

We acknowledge the people responsible for generating the data from reference sources included

in this manuscript.

AUTHORSHIP CONTRIBUTIONS

Participated in research design: Lin, Wong

Conducted experiments: Lin, Wong

Performed data analysis: Lin, Wong, Wright, Hop

Wrote or contributed to the writing of the manuscript: Lin, Wong, Wright, Hop

REFERENCES

Benet LZ, and Zia-Amirhosseini P (1995) Basic Principles of Pharmacokinetics. *Toxicol Pathol* **23**:115–123, SAGE Publications Inc.

Boxenbaum H (1984) Interspecies pharmacokinetic scaling and the evolutionary-comparative paradigm. *Drug Metab Rev* **15**:1071–1121, England.

Chen C, Fancher RM, Chimalakonda A, Rodrigues AD, Marathe P, Yang Z, and others (2008) Determination of Hepatic Blood Flow in Cynomolgus Monkeys Using Indocyanine Green Coupled with a Sensitive LC/MS/MS Method, in *2nd Asian Pacific Regional ISSX2nd Asian Pacific Regional ISSX Meeting (国际药物学会第二届亚太地区会议)* pp 61–62, 国际药物代谢学会.

Chiang P-C, La H, Zhang H, and Wong H (2013) Systemic Concentrations Can Limit the Oral Absorption of Poorly Soluble Drugs: An Investigation of Non-Sink Permeation Using Physiologically Based Pharmacokinetic Modeling. *Mol Pharmaceutics* **10**:3980–3988, American Chemical Society.

Chung J, Alvarez-Nunez F, Chow V, Daurio D, Davis J, Dodds M, Emery M, Litwiler K, Paccaly A, Peng J, Rock B, Wienkers L, Yang C, Yu Z, and Wahlstrom J (2015) Utilizing Physiologically Based Pharmacokinetic Modeling to Inform Formulation and Clinical Development for a Compound with pH-Dependent Solubility. *Journal of Pharmaceutical Sciences* **104**:1522–1532.

Darwich AS, Margolskee A, Pepin X, Aarons L, Galetin A, Rostami-Hodjegan A, Carlert S, Hammarberg M, Hilgendorf C, Johansson P, Karlsson E, Murphy D, Tannergren C, Thörn H, Yasin M, Mazuir F, Nicolas O, Ramusovic S, Xu C, Pathak SM, Korjamo T, Laru J, Malkki J, Pappinen S, Tuunainen J, Dressman J, Hansmann S, Kostewicz E, He H, Heimbach T, Wu F, Hoft C, Pang Y, Bolger MB, Huehn E, Lukacova V, Mullin JM, Szeto KX, Costales C, Lin J, McAllister M, Modi S, Rotter C, Varma M, Wong M, Mitra A, Bevernage J, Biewenga J, Van Peer A, Lloyd R, Shardlow C, Langguth P, Mishenzon I, Nguyen MA, Brown J, Lennernäs H, and Abrahamsson B (2017) IMI – Oral biopharmaceutics tools project – Evaluation of bottom-up PBPK prediction success part 3: Identifying gaps in system parameters by analysing In Silico performance across different compound classes. *European Journal of Pharmaceutical Sciences* **96**:626–642.

Davies B, and Morris T (1993) Physiological parameters in laboratory animals and humans. *Pharm Res* **10**:1093–1095.

Di L, and Obach RS (2015) Addressing the Challenges of Low Clearance in Drug Research. *AAPS J* **17**:352–357.

Di L, Trapa P, Obach RS, Atkinson K, Bi Y-A, Wolford AC, Tan B, McDonald TS, Lai Y, and Tremaine LM (2012) A Novel Relay Method for Determining Low-Clearance Values. *Drug Metab Dispos* **40**:1860–1865, American Society for Pharmacology and Experimental Therapeutics.

Dlugosz A, Agrawal S, and Kirkpatrick P (2012) Vismodegib. *Nature Reviews Drug Discovery* **11**:437–438.

Dolton MJ, Chiang P-C, Ma F, Jin JY, and Chen Y (2020) A Physiologically Based Pharmacokinetic Model of Vismodegib: Deconvoluting the Impact of Saturable Plasma Protein Binding, pH-Dependent Solubility and Nonsink Permeation. *AAPS J* **22**:117.

Drevon D, Fursa SR, and Malcolm AL (2017) Intercoder Reliability and Validity of WebPlotDigitizer in Extracting Graphed Data. *Behav Modif* **41**:323–339, SAGE Publications Inc.

Ferraris RP, Lee PP, and Diamond JM (1989) Origin of regional and species differences in intestinal glucose uptake. *American Journal of Physiology-Gastrointestinal and Liver Physiology* **257**:G689–G697.

Gibaldi Milo, and Perrier Donald (1982) Pharmacokinetics / Milo Gibaldi, Donald Perrier, Marcel Dekker New York.

Graham RA, Hop CECA, Borin MT, Lum BL, Colburn D, Chang I, Shin YG, Malhi V, Low JA, and Dresser MJ (2012) Single and multiple dose intravenous and oral pharmacokinetics of the hedgehog pathway inhibitor vismodegib in healthy female subjects. *British Journal of Clinical Pharmacology* **74**:788–796.

Graham RA, Lum BL, Cheeti S, Jin JY, Jorga K, Von Hoff DD, Rudin CM, Reddy JC, Low JA, and LoRusso PM (2011) Pharmacokinetics of Hedgehog Pathway Inhibitor Vismodegib (GDC-0449) in Patients with Locally Advanced or Metastatic Solid Tumors: the Role of Alpha-1-Acid Glycoprotein Binding. *Clin Cancer Res* **17**:2512–2520.

Grimstein M, Yang Y, Zhang X, Grillo J, Huang S-M, Zineh I, and Wang Y (2019) Physiologically Based Pharmacokinetic Modeling in Regulatory Science: An Update From the U.S. Food and Drug Administration's Office of Clinical Pharmacology. *Journal of Pharmaceutical Sciences* **108**:21–25.

Hall C, Lueshen E, Mosat A, and Linninger A (2012) Interspecies Scaling in Pharmacokinetics: A Novel Whole-Body Physiologically Based Modeling Framework to Discover Drug Biodistribution Mechanisms in vivo. *Journal of pharmaceutical sciences* **101**:1221–41.

Helander HF, and Fändriks L (2014) Surface area of the digestive tract – revisited. *Scandinavian Journal of Gastroenterology* **49**:681–689, Taylor & Francis.

Huang Q, and Riviere JE (2014) The application of allometric scaling principles to predict pharmacokinetic parameters across species. *Expert Opinion on Drug Metabolism & Toxicology* **10**:1241–1253, Taylor & Francis.

Ikegami K, Tagawa K, Narisawa S, and Osawa T (2003) Suitability of the Cynomolgus Monkey as an Animal Model for Drug Absorption Studies of Oral Dosage Forms from the Viewpoint of Gastrointestinal Physiology. *Biological and Pharmaceutical Bulletin* **26**:1442–1447.

Jamzad S, and Fassihi R (2006) Role of surfactant and pH on dissolution properties of fenofibrate and glipizide—A technical note. *AAPS PharmSciTech* **7**:E17–E22.

Jones H, Chen Y, Gibson C, Heimbach T, Parrott N, Peters S, Snoeys J, Upreti V, Zheng M, and Hall S (2015) Physiologically based pharmacokinetic modeling in drug discovery and development: A pharmaceutical industry perspective. *Clin Pharmacol Ther* **97**:247–262.

Jones HM, Mayawala K, and Poulin P (2012) Dose Selection Based on Physiologically Based Pharmacokinetic (PBPK) Approaches. *AAPS J* **15**:377–387.

Jones HM, Parrott N, Ohlenbusch G, and Lavé T (2006) Predicting Pharmacokinetic Food Effects Using Biorelevant Solubility Media and Physiologically Based Modelling. *Clin Pharmacokinet* **45**:1213–1226.

Kararli TT (1995) Comparison of the gastrointestinal anatomy, physiology, and biochemistry of humans and commonly used laboratory animals. *Biopharm Drug Dispos* **16**:351–380.

Kondo H, Takahashi Y, Watanabe T, Yokohama S, and Watanabe J (2003) Gastrointestinal transit of liquids in unfed cynomolgus monkeys. *Biopharmaceutics & Drug Disposition* **24**:131–140.

Li X, Shi L, Tang X, Wang Q, Zhou L, Song W, Feng Z, Ge J, Li JK, Yang L, Wen A, and Zhang Y (2017) Mechanistic prediction of food effects for Compound A tablet using PBPK model. *Saudi J Biol Sci* **24**:603–609.

Lin JH (1998) Applications and Limitations of Interspecies Scaling and In Vitro Extrapolation in Pharmacokinetics. *Drug Metab Dispos* **26**:1202–1212, American Society for Pharmacology and Experimental Therapeutics.

Lin L, and Wong H (2017) Predicting Oral Drug Absorption: Mini Review on Physiologically-Based Pharmacokinetic Models. *Pharmaceutics* **9**:41.

Liu P, De Wulf O, Laru J, Heikkilä T, van Veen B, Kiesvaara J, Hirvonen J, Peltonen L, and Laaksonen T (2013) Dissolution Studies of Poorly Soluble Drug Nanosuspensions in Non-sink Conditions. *AAPS PharmSciTech* **14**:748–756.

LoRusso PM, Rudin CM, Reddy JC, Tibes R, Weiss GJ, Borad MJ, Hann CL, Brahmer JR, Chang I, Darbonne WC, Graham RA, Zerivitz KL, Low JA, and Hoff DDV (2011) Phase I Trial of Hedgehog Pathway Inhibitor Vismodegib (GDC-0449) in Patients with Refractory, Locally Advanced or Metastatic Solid Tumors. *Clin Cancer Res* **17**:2502–2511, American Association for Cancer Research.

31

Lu T, Wang B, Gao Y, Dresser M, Graham RA, and Jin JY (2015) Semi-Mechanism-Based Population Pharmacokinetic Modeling of the Hedgehog Pathway Inhibitor Vismodegib. *CPT: Pharmacometrics & Systems Pharmacology* **4**:680–689.

Maharaj A, Fotaki N, and Edginton A (2015) Parameterization of small intestinal water volume using PBPK modeling. *European Journal of Pharmaceutical Sciences* **67**:55–64.

Mandikian D, Figueroa I, Oldendorp A, Rafidi H, Ulufatu S, Schweiger MG, Couch JA, Dybdal N, Joseph SB, Prabhu S, Ferl GZ, and Boswell CA (2018) Tissue Physiology of Cynomolgus Monkeys: Cross-Species Comparison and Implications for Translational Pharmacology. *AAPS J* **20**:107.

Margolskee A, Darwich AS, Pepin X, Aarons L, Galetin A, Rostami-Hodjegan A, Carlert S, Hammarberg M, Hilgendorf C, Johansson P, Karlsson E, Murphy D, Tannergren C, Thörn H, Yasin M, Mazuir F, Nicolas O, Ramusovic S, Xu C, Pathak SM, Korjamo T, Laru J, Malkki J, Pappinen S, Tuunainen J, Dressman J, Hansmann S, Kostewicz E, He H, Heimbach T, Wu F, Hoft C, Laplanche L, Pang Y, Bolger MB, Huehn E, Lukacova V, Mullin JM, Szeto KX, Costales C, Lin J, McAllister M, Modi S, Rotter C, Varma M, Wong M, Mitra A, Bevernage J, Biewenga J, Van Peer A, Lloyd R, Shardlow C, Langguth P, Mishenzon I, Nguyen MA, Brown J, Lennernäs H, and Abrahamsson B (2017) IMI – Oral biopharmaceutics tools project – Evaluation of bottom-up PBPK prediction success part 2: An introduction to the simulation exercise and overview of results. *European Journal of Pharmaceutical Sciences* **96**:610–625.

Matsumura N, Ono A, Akiyama Y, Fujita T, and Sugano K (2020) Bottom-Up Physiologically Based Oral Absorption Modeling of Free Weak Base Drugs. *Pharmaceutics* **12**:844, Multidisciplinary Digital Publishing Institute.

Noyes AA, and Whitney WR (1897) THE RATE OF SOLUTION OF SOLID SUBSTANCES IN THEIR OWN SOLUTIONS. *J Am Chem Soc* **19**:930–934.

Parrott N, Hainzl D, Alberati D, Hofmann C, Robson R, Boutouyrie B, and Martin-Facklam M (2013) Physiologically Based Pharmacokinetic Modelling to Predict Single- and Multiple-Dose Human Pharmacokinetics of Bitopertin. *Clin Pharmacokinet* **52**:673–683.

Peters SA (2008) Evaluation of a Generic Physiologically Based Pharmacokinetic Model for Lineshape Analysis. *Clin Pharmacokinet* **47**:261–275.

Poulin P, Jones RDO, Jones HM, Gibson CR, Rowland M, Chien JY, Ring BJ, Adkison KK, Ku MS, He H, Vuppugalla R, Marathe P, Fischer V, Dutta S, Sinha VK, Björnsson T, Lavé T, and Yates JWT (2011) PHRMA CPCDC initiative on predictive models of human pharmacokinetics, part 5: prediction of plasma concentration-time profiles in human by using the physiologically-based pharmacokinetic modeling approach. *J Pharm Sci* **100**:4127–4157.

Rabot S, Viso M, Martin F, Blanquie J-P, Popot F, Bensaada M, Vaissade P, Searby N, and Szylit O (1997) Effects of chair-restraint on gastrointestinal transit time and colonic

32

fermentation in male rhesus monkey (Macaca mulatta). *Journal of Medical Primatology*
26:190–195.

Rohatgi, Ankit (2020) *WebPlotDigitizer*, Pacifica, California, USA.

Rudin CM (2012) Vismodegib. *Clin Cancer Res* **18**:3218–3222, American Association for
Cancer Research.

Sager JE, Yu J, Ragueneau-Majlessi I, and Isoherranen N (2015) Physiologically Based
Pharmacokinetic (PBPK) Modeling and Simulation Approaches: A Systematic Review of
Published Models, Applications, and Model Verification. *Drug Metab Dispos* **43**:1823–
1837.

Sugano K, Okazaki A, Sugimoto S, Tavornvipas S, Omura A, and Mano T (2007) Solubility and
dissolution profile assessment in drug discovery. *Drug Metab Pharmacokinet* **22**:225–
254.

Willmann S, Edginton AN, and Dressman JB (2007) Development and Validation of a
Physiology-based Model for the Prediction of Oral Absorption in Monkeys. *Pharm Res*
24:1275–1282.

Wong H, Alicke B, West KA, Pacheco P, La H, Januario T, Yauch RL, de Sauvage FJ, and
Gould SE (2011) Pharmacokinetic–pharmacodynamic analysis of vismodegib in
preclinical models of mutational and ligand-dependent Hedgehog pathway activation.
Clinical Cancer Research **17**:4682–4692, AACR.

Wong H, Chen JZ, Chou B, Halladay JS, Kenny JR, La H, Marsters JC, Plise E, Rudewicz PJ,
Robarge K, Shin Y, Wong S, Zhang C, and Khojasteh SC (2009) Preclinical assessment
of the absorption, distribution, metabolism and excretion of GDC-0449 (2-chloro-N-(4-
chloro-3-(pyridin-2-yl)phenyl)-4-(methylsulfonyl)benzamide), an orally bioavailable
systemic Hedgehog signalling pathway inhibitor. *Xenobiotica* **39**:850–861.

Wong H, Theil F-P, Cui Y, Marsters JC, Khojasteh SC, Vernillet L, La H, Song X, Wang H,
Morinello EJ, Deng Y, and Hop CECA (2010) Interplay of Dissolution, Solubility, and
Nonsink Permeation Determines the Oral Absorption of the Hedgehog Pathway Inhibitor
GDC-0449 in Dogs: An Investigation Using Preclinical Studies and Physiologically
Based Pharmacokinetic Modeling. *Drug Metab Dispos* **38**:1029–1038, American Society
for Pharmacology and Experimental Therapeutics.

Yamazaki S, Skaptason J, Romero D, Vekich S, Jones HM, Tan W, Wilner KD, and
Koudriakova T (2011) Prediction of Oral Pharmacokinetics of cMet Kinase Inhibitors in
Humans: Physiologically Based Pharmacokinetic Model Versus Traditional One-
Compartment Model. *Drug Metab Dispos* **39**:383–393.

Zhang X, Duan J, Kesisoglou F, Novakovic J, Amidon GL, Jamei M, Lukacova V, Eissing T,
Tsakalozou E, Zhao L, and Lionberger R (2017) Mechanistic Oral Absorption Modeling
and Simulation for Formulation Development and Bioequivalence Evaluation: Report of
an FDA Public Workshop. *CPT: Pharmacometrics & Systems Pharmacology* **6**:492–495.

Zhuang X, and Lu C (2016) PBPK modeling and simulation in drug research and development. *Acta Pharmaceutica Sinica B* **6**:430–440.

FOOTNOTES

HW is an employee of the University of British Columbia and is a consultant for Genentech.

MRW and CECAH are employees of Genentech.

Send reprint requests to: Harvey Wong, Faculty of Pharmaceutical Sciences, The University of British Columbia, 2405 Wesbrook Mall, Vancouver, BC. V6T 1Z3, Canada E-mail: harvey.wong@ubc.ca

FIGURE LEGENDS

Figure 1: The PBPK model structure used in this study characterizes the gut into nine compartments with an undissolved and dissolved section for each. The nine compartments consist of a stomach, seven small intestinal segments (SI1-7), and a colon. Flow through these segments is dictated by rate constants (Kt.stom for gastric emptying, Kt1-7 for intestinal flow, and Kt.colon for colonic excretion). Dissolved drug can permeate into the liver, which is connected to body via hepatic blood flow (Q_h). Elimination occurs in the liver, determined by fraction unbound (f_u) and intrinsic clearance (Cl_{int}).

Figure 2: Preclinical concentration-time profiles for single IV (A,C,E) and single PO (B,D,E) dose in rat (A,B), dog (C,D), and monkey (E,F). Lines represent PBPK simulations and squares represent observed data points.

Figure 3: Predicted oral human PK profile using PBPK model driven by predicted human pharmacokinetics and observed data. Single dose profiles (left) and multiple dose profiles (right) for 150, 270, and 540 mg. Multiple daily doses were given after a 7-day washout following a single oral dose. Lines represent simulations and symbols represent observed data points.

Figure 4: Predicted oral human PK profile from PBPK model driven by observed pharmacokinetics in human and observed data. Single dose profile (left) and multiple dose

36

profiles (right) for 150, 270, and 540 mg. Multiple daily doses were given after a 7-day washout following a single oral dose. Lines represent simulations and symbols represent observed data points.

Figure 5: Fitted (Single Dose) and Predicted (Multiple Dose) oral human PK profile using a one-compartment model. Models were fit to single dose data (left) and then used to simulate multiple dose profiles (right). Multiple daily doses were given after a 7-day washout following a single oral dose. Lines represent simulations and symbols represent observed data points.

Figure 6: Permeation gradient factors (PGF) in the PBPK model for single dose (day 1) (left) and following multiple doses to steady-state (right). The PGF, which measures the concentration gradient between unbound concentrations in the gut and in the liver, analyzes the magnitude of the nonsink effect on permeation. A PGF of 0.67 - 1.0 indicates sink conditions, meaning the concentration gradient between unbound intestinal concentrations and unbound concentrations in the liver has an inconsequential effect on permeation.

Figure 7: Comparing the oral human PK profile for 150 mg in PBPK models with sink (dashed line) and nonsink (solid line) conditions enabled for permeability. The sink model omits the concentration gradient between unbound intestinal concentrations and unbound liver concentrations that drive permeation. Dashed line represents sink permeability model, solid line represents nonsink permeability model, and circles represent observed data.

Figure 8: A sensitivity analysis showing changes in simulated vismodegib systemic

concentrations over a 10-fold increase in intestinal solubility (C_{sol_IF}).

TABLES

Table 1: Species specific and select compound specific parameters for PBPK model input.

Species Specific Model Parameters				
	Sprague-Dawley Rat	Beagle Dog	Cynomolgus Monkey	Human
Body Weight (kg)	0.25	9.0	3.5	70
Stomach Transit Rate Constant (Kt.stom) (h^{-1})	4[1]	4[4]	0.73[5]	4[12]
Intestinal Transit Rate Constant (Kt) (h^{-1})[a]	4.76[1]	3.85[4]	2.59[6]	3.84, 1.06, 1.35, 1.72, 2.38, 3.44, 0.23[12]
Colon Transit Rate Constant (Kt.colon) (h^{-1})	0.017[1]	0.083[4]	0.023[e,16]	0.077[12]
Stomach Volume (mL)	3.4[1]	450[4]	100[7]	450[12]
Intestinal Length (L) (cm)[b]	17.01, 12.53, 9.23, 6.80, 5.01, 3.69, 2.72[1]	44.76, 32.98, 24.3, 17.9, 13.19, 9.72, 7.16[4]	25, 30, 40, 37.5, 37.5, 37.5, 37.5[7,8]	14.58, 60.26, 60.26, 60.26, 60.26, 60.26, 13.5[12]
Intestinal Radius (r) (cm)	0.2[1]	0.5[4]	0.2[7]	1.25[13]
Liver Volume (mL)[c]	10[2]	432[2]	94.5[2]	1695[2]
Hepatic Blood Flow (Q$_h$) (mL/min/kg)	55.2[2]	30.8[2]	31.7[d,2,9,10,11]	21.4[14]
Volume of Distribution (Vd) (L)	0.122[3]	9.572[3]	3.44[3]	Predicted: 53.6[3] Observed: 16.4[15]
Intrinsic Clearance (Clint) (mL/min/kg)	0.329[3]	6.28[3]	1142[3]	Predicted: 3.21[3] Observed: 0.344[15]
Fraction Unbound (fu)	0.0154[3]	0.042[3]	0.043[3]	0.03[3]

[a] Values listed for humans are written for transit in order from proximal to distal small intestinal compartment..[b]Small intestinal lengths are written in order from proximal to distal small intestinal segment, for use in calculating surface area and volume. Duodenum, jejunum, and

ileum proportions in monkeys were reportedly similar to humans, so total intestinal length was divided into seven segments similarly. Total small intestinal volume in humans was set to 116 mL and each segment is proportioned accordingly (Maharaj *et al.*, 2015). [c]Liver volumes for dog and monkey were adjusted for body weight. [d]Monkey hepatic blood flow used is an average of reported values. [e]Monkey colon transit time was calculated by subtracting mean stomach and small intestine residence time from mean total gut residence time.

[1] (Chiang *et al.*, 2013), [2](Davies and Morris, 1993), [3](Wong *et al.*, 2009), [4](Wong *et al.*, 2010), [5](Kondo *et al.*, 2003), [6](Ikegami *et al.*, 2003), [7](Kararli, 1995), [8](Willmann *et al.*, 2007), [9](Chen *et al.*, 2008) , [10](Hall *et al.*, 2012) , [11](Mandikian *et al.*, 2018), [12](Li *et al.*, 2017), [13](Helander and Fändriks, 2014), [14](Jones *et al.*, 2006), [15](Graham *et al.*, 2012), [16](Rabot *et al.*, 1997)

Table 2: Predicted and observed PK parameters for preclinical species for IV and PO dose.

	PK Parameter	Sprague-Dawley Rat				Beagle Dog				Cynomolgus Monkey			
		PBPK	Observed	Fold Error	Lineshape Fold Error	PBPK	Observed	Fold Error	Lineshape Fold Error	PBPK	Observed	Fold Error	Lineshape Fold Error
IV Dose	$AUC_{0\text{-}inf}$ (µM*h)	8.49	9.45	1.11	1.13	145	142	1.02	1.13	2.03	2.27	1.19	1.22
	C_{max} (µM)	4.45	5.36	1.20		2.22	3.36	1.51		2.28	2.25	1.01	
PO Dose	$AUC_{0\text{-}inf}$ (µM*h)	11.2	24.9	2.22	6.09	93.6	93.5	1.00	1.28	1.09	0.61	1.78	2.06
	C_{max} (µM)	4.08	6.55	1.61		1.28	1.40	1.09		0.326	0.38	1.17	
	t_{max} (h)	0.884	0.667	1.33		2.00	9.33	4.66		1.79	2.00	1.18	

$AUC_{0\text{-}inf}$, area under the concentration-time curve extrapolated to infinity; C_{max}, maximum concentration; t_{max}, time to maximum concentration.

Table 3: Predicted human PK parameters genera ted from the PBPK model driven by predicted human pharmacokinetics (from allometry) compared to observed values for 150, 270, and 540 mg single and multiple doses.

	Parameter	150 mg				270 mg				540 mg			
		PBPK (predicted human PK)	Obs	Fold Error	Lineshape Fold Error	PBPK (predicted human PK)	Obs	Fold Error	Lineshape Fold error	PBPK (predicted human PK)	Obs	Fold Error	Lineshape Fold Error
Single Dose	C_{max} (µM)	1.07	3.25	3.04	2.88	1.59	6.96	4.38	4.04	2.47	6.60	2.67	2.48
	AUC_{0-168} (µM*h)	105	482	4.59		156	974	6.24		243	1017	4.19	
Multiple Dose	C_{max} (µM)	5.76	23.0	3.99	4.37	7.94	20.7	2.61	2.90	11.0	22.2	2.02	2.18
	AUC_{ss} (µM*h)	129	503	3.90		179	427	2.39		248	473	1.91	

AUC_{0-168}, area under the concentration-time curve from 0h to 168 h postdose; AUC_{ss}, area under the concentration-time curve from 0 h to 24 h postdose at steady state; C_{max}, maximum concentration; Obs, observed values

42

Table 4: Predicted human PK parameters generated from the PBPK model driven by clinically observed human pharmacokinetics compared to observed values for 150, 270, and 540 mg single and multiple doses.

	Parameter	150 mg				270 mg				540 mg			
		PBPK (Clinical Input)	Obs	Fold Error	Lineshape Fold Error	PBPK (Clinical Input)	Obs	Fold Error	Lineshape Fold error	PBPK (Clinical Input)	Obs	Fold Error	Lineshape Fold Error
Single Dose	C_{max} (µM)	3.24	3.25	1.00	1.37	4.72	6.96	1.47	1.48	7.12	6.60	1.08	1.46
	AUC_{0-168} (µM*h)	441	482	1.09		642	974	1.52		970	1017	1.05	
Multiple Dose	C_{max} (µM)	22.0	23.0	1.05	1.08	24.5	20.7	1.18	1.16	26.7	22.2	1.20	1.23
	AUC_{ss} (µM*h)	515	503	1.02		573	427	1.34		625	473	1.32	

AUC_{0-168}, area under the concentration-time curve from 0h to 168 h postdose; AUC_{ss}, area under the concentration-time curve from 0 h to 24 h postdose at steady state; C_{max}, maximum concentration; Obs, observed values

43

Table 5: Fitted (single dose) and Predicted (multiple dose) human PK parameters generated using the one-compartment model compared to observed values for 150, 270, and 540 mg single and multiple doses.

		150 mg				270 mg				540 mg			
	Parameter	1 Comp.	Obs	Fold Error	Lineshape Fold Error	1 Comp.	Obs	Fold Error	Lineshape Fold error	1 Comp.	Obs	Fold Error	Lineshape Fold Error
Single Dose	C_{max} (µM)	2.80	3.25	*fitted[a]*	*fitted[a]*	5.46	6.96	*fitted[a]*	*fitted[a]*	6.18	6.60	*fitted[a]*	*fitted[a]*
Single Dose	AUC_{0-168} (µM*h)	403	482	*fitted[a]*	*fitted[a]*	787	974	*fitted[a]*	*fitted[a]*	893	1017	*fitted[a]*	*fitted[a]*
Multiple Dose	C_{max} (µM)	56.8	23.0	2.47	1.77	111	20.7	5.36	3.83	126	22.2	5.68	3.88
Multiple Dose	AUC_{ss} (µM*h)	1349	503	2.68	1.77	2638	427	6.18	3.83	2983	473	6.31	3.88

AUC_{0-168}, area under the concentration-time curve from 0h to 168 h postdose; AUC_{ss}, area under the concentration-time curve from 0 h to 24 h postdose at steady state; C_{max}, maximum concentration; Obs, observed values
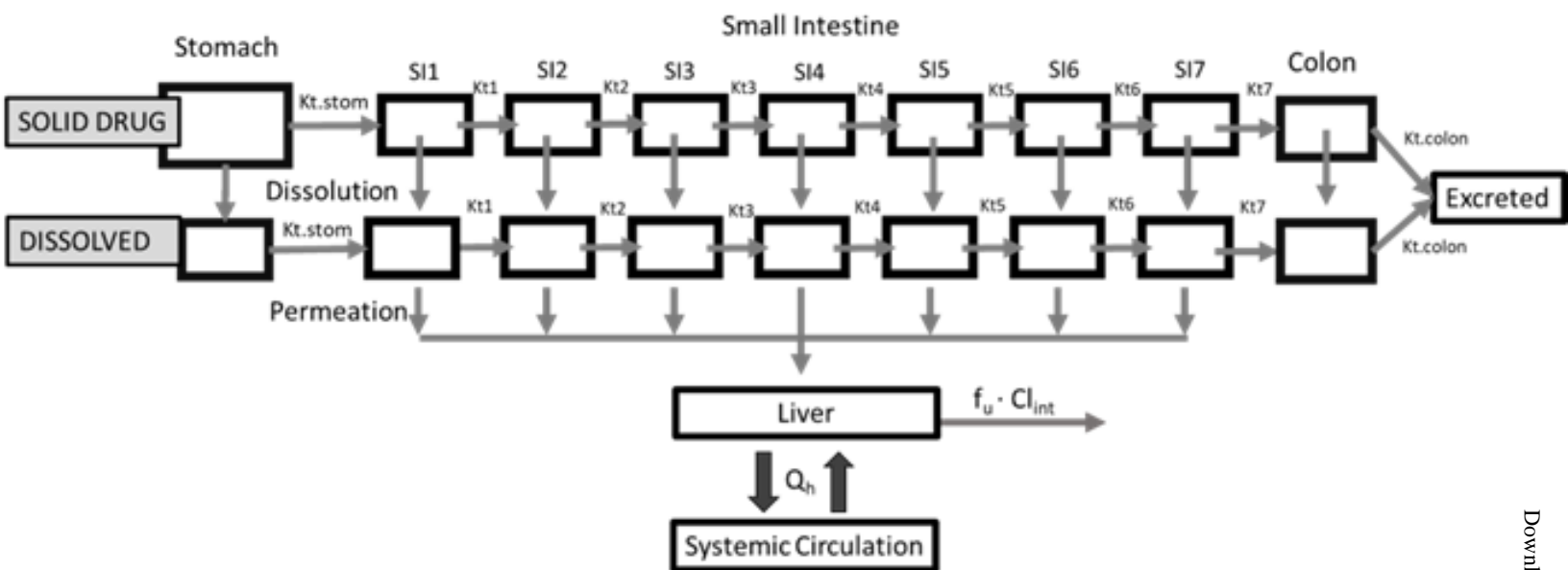
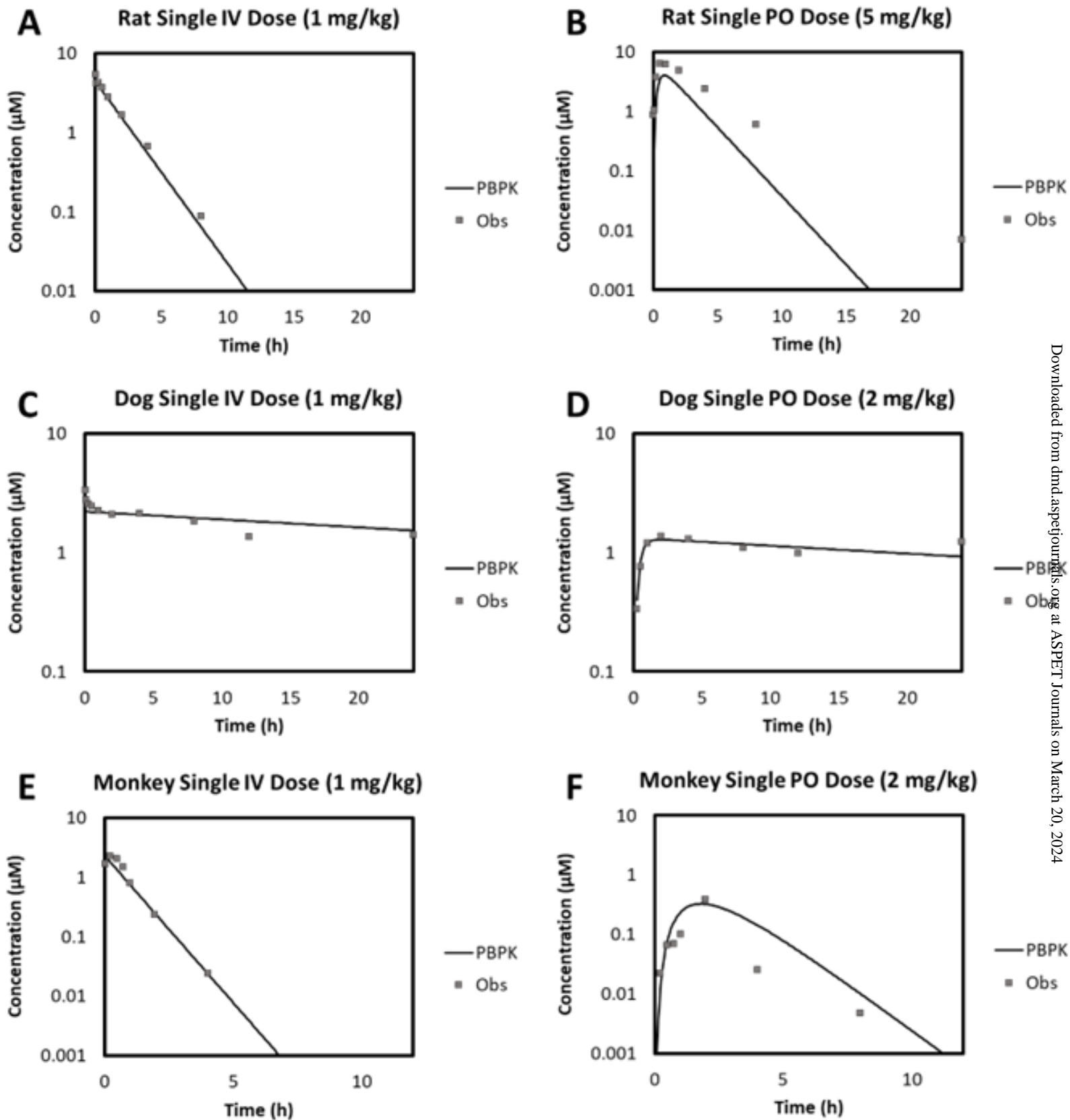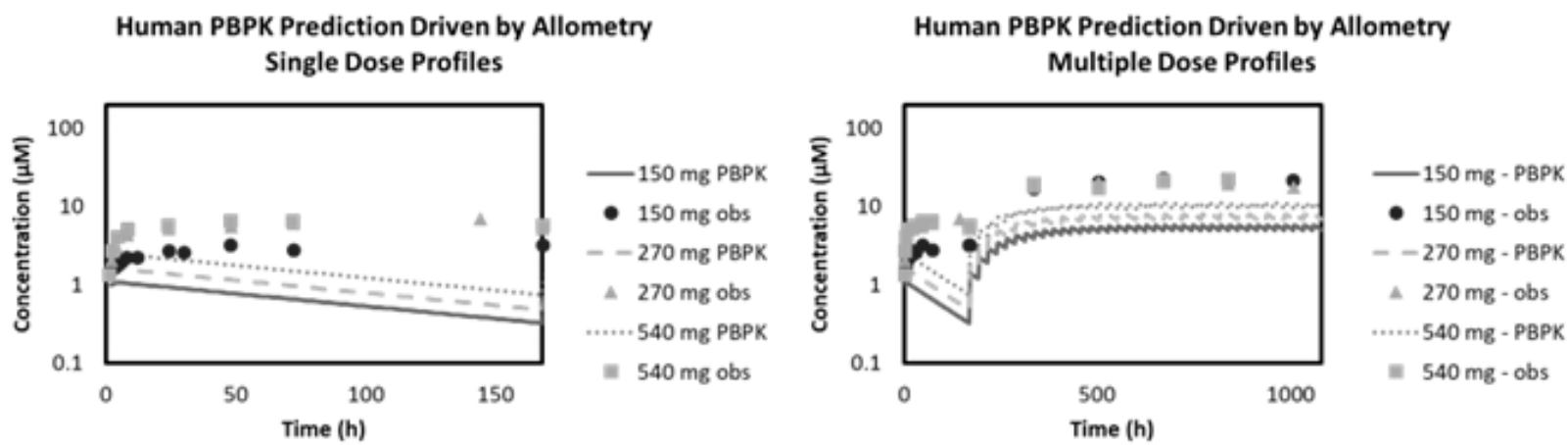[a] One-compartment models were fitted to observed single dose data.

44
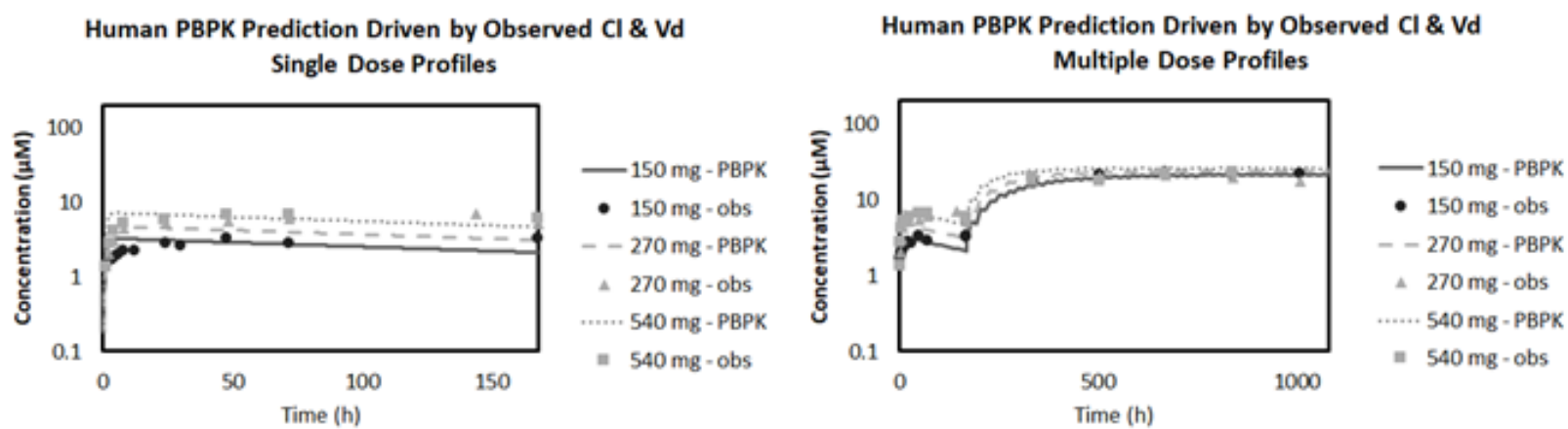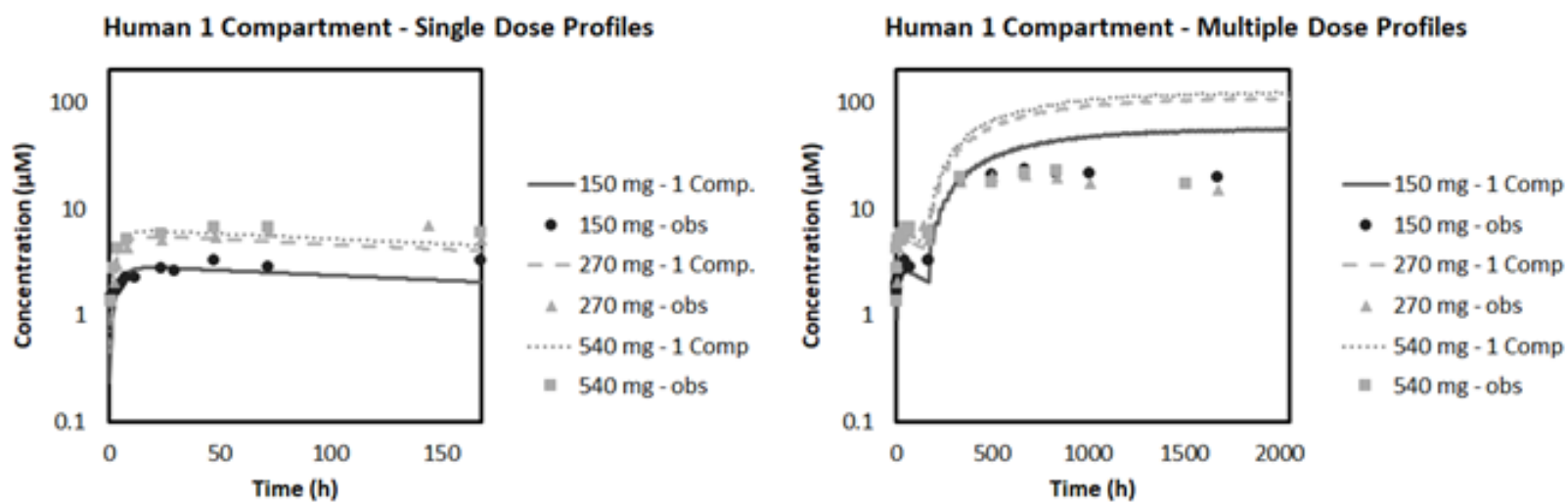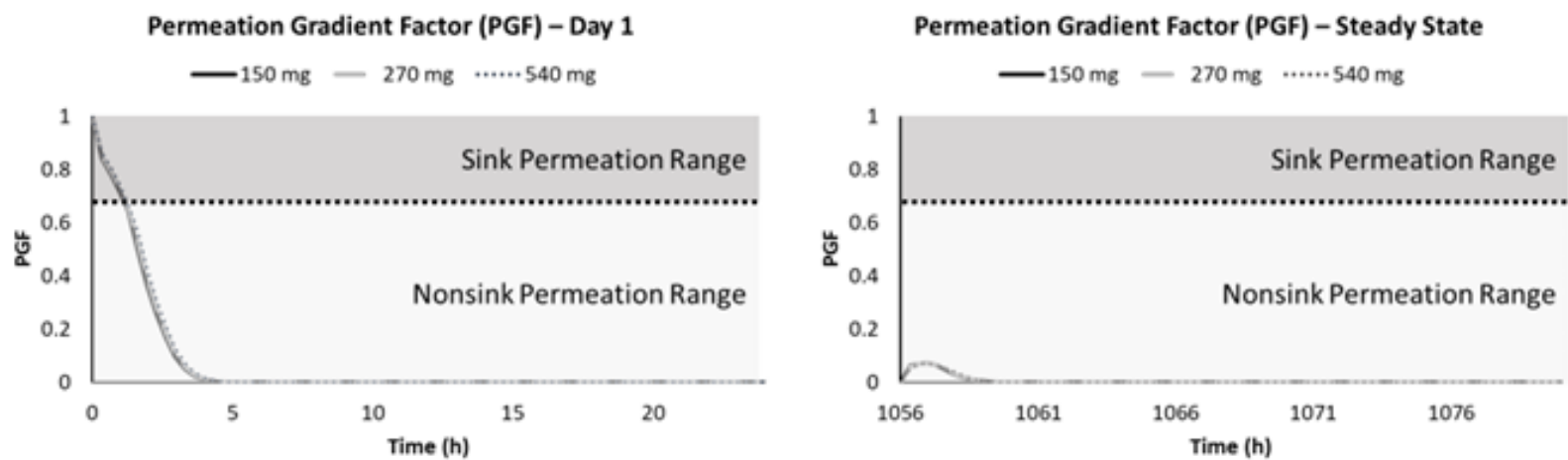
Figure 1

Figure 2

Figure 3

Figure 4

Figure 5

Figure 6

Sink vs. Nonsink PBPK Models (150 mg)

-----Sink Permeability ——Nonsink Permeability ◉ Observed

Figure 7

Sensitivity of Vismodegib Concentrations to Intestinal Solubility (C_{sol_IF})

Figure 8